THE JOURNAL OF PHYSICAL CHEMISTRY C LETTERS

2008, *112,* 13311–13316
Published on Web 08/13/2008

Catalytic Behavior of Individual Au Nanocrystals in the Local Anodic Oxidation of Si Surfaces

T. Vijaykumar,[†] Gargi Raina,[‡] Stefan Heun,[§] and G. U. Kulkarni*,[†]

Chemistry and Physics of Materials Unit and DST Unit on Nanoscience, Jawaharlal Nehru Centre for Advanced Scientific Research, Jakkur P.O., Bangalore 560 064, India, School of Electrical Sciences, Vellore Institute of Technology, Vellore 632014, India, and NEST CNR-INFM and Scuola Normale Superiore, Piazza San Silvestro 12, 56127, Pisa, Italy

Received: May 22, 2008; Revised Manuscript Received: July 25, 2008

Local anodic oxidation (LAO) of Si surfaces deposited with Au nanoislands by electroless plating and Au nanocrystals (∼3 nm) by spin coating has been carried out using a biased AFM tip. Isolated nanoislands and individual nanocrystals exhibited high catalytic activity producing oxide patterns with a height above 13 and 40 nm, respectively, in contrast to 2.5 nm high patterns observed on bare portions of the Si surface. Au nanocrystal aggregates also present on the surface exhibited relatively less activity compared to single nanocrystals. In the case of Au nanocrystal dispersion on the Si surface, etch patterns obtained after a HF wash exhibited depths of 13 and 8 nm with respect to the locations of single nanocrystal and the aggregate, respectively, compared to ∼2 nm trench depth from LAO on the bare surface. Further, nanocrystal-induced etch patterns were much narrower, ∼12 nm. In another experiment, a Au-deposited tip catalytically induced LAO on the bare Si surface with features of ∼6 nm height and the corresponding trenches of ∼2.2 nm.

Introduction

The catalytic activity of gold nanocrystals is an active area of research since the first report by Haruta et al. in 1986.[1−5] There has been intense activity especially in the past few years[6,7] not only to produce new formulations of Au catalysts[8] and to apply them in new processes,[9,10] but also to understand this interesting catalytic phenomenon.[11,12] The Au surface is thought to be nobler than the bulk,[13] yet it is the surface which becomes catalytically active when the Au crystal size is reduced to the nanoscale, especially at oxide interfaces such as SiO_2,[14,15] Al_2O_3,[16,17] or CeO_2.[18] Additionally, $LaPO_4$ has also been used as a support.[8]

Gold catalysts have been popular in oxidative conversion of carbon monoxide,[1] a reaction of immense importance in pollution control. Its origin has been a subject matter of several experimental and theoretical investigations. Guzman et al.[19] used X-ray absorption spectroscopy to characterize the average cluster size and identify the oxidation states of Au. On the basis of scanning tunneling spectroscopy, Goodman and co-workers[11] attributed the catalytic activity of Au deposited on TiO_2 to the quantum size effect associated with the Au clusters. Using density functional theory, Lopez and Nørskov have calculated the adsorption energy of CO and O on a number of different gold surfaces. It transpires that small clusters of the metal, unlike close packed gold surfaces, can form strong bonds to a variety of adsorbates, including CO, H_2, and O_2. Thus, it is generally accepted that Au atoms at steps and corners on the surface of nanocrystals have a lower coordination number and possess d states that are closer to the Fermi level. These atoms lacking complete metallic character can activate oxygen at an oxide interface leading to catalytic action.[20] There have been landmark studies on other metal clusters, for instance, on Pd clusters by Heiz et al.[21] who showed that the particle surface and its electronic structure are responsible for the size dependent catalytic properties. Similar experiments have been carried out on Pt and Au clusters as well.[1,8,11,12,22]

In this paper, we report our results on the catalytic action of Au nanocrystals in the oxidation of Si. Previously, patterned Au films have been used for selective oxidation of Si surfaces.[23,24] In this study, we have carried out selective oxidation using a conducting atomic force microscope (AFM) tip in a process commonly known as local anodic oxidation (LAO). In LAO, a negative bias of few volts applied between the conducting tip and the grounded substrate produces an intense but confined electric field inducing local oxidation. This is believed to be mediated by a water meniscus condensed from the ambient humidity.[25] The water meniscus formed between the tip and the sample surface is the electrolyte. When a negative bias is applied to the tip, the OH^- ions contained in the water meniscus are driven to the sample surface by the electric field, and localized anodic oxidation of the sample occurs beneath the tip apex, resulting in the growth of oxide structures. The oxidation is marked by the outgrowth of the oxide due to volume expansion and is more facile at relative humidity values above 35%.[26] The amount of silicon consumed in the process can be determined by etching away the oxide to create a trench. The extent of oxidation is thus measurable in terms of the protrusion of the oxide and the depth of the trench. LAO has emerged as an important lithographic technique for nanoscale

* To whom correspondence should be addressed. E-mail: kulkarni@jncasr.ac.in.
[†] Jawaharlal Nehru Centre for Advanced Scientific Research.
[‡] Vellore Institute of Technology.
[§] NEST CNR-INFM and Scuola Normale Superiore.

10.1021/jp804545s CCC: $40.75

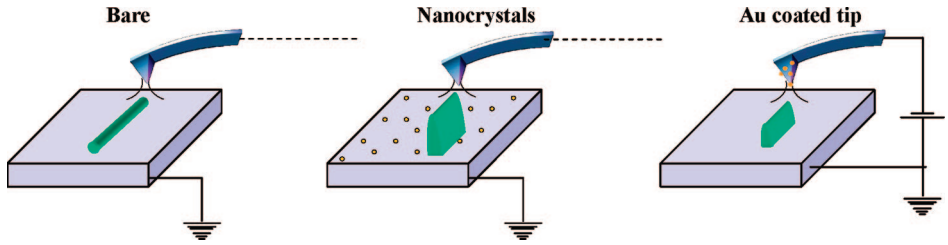

Figure 1. LAO on bare Si (left), Au nanocrystal loaded Si substrate (middle), and on bare Si using a tip coated with Au nanocrystals (right).

oxide patterning of metal and semiconductor surfaces.[27] Recently, a sputtered nanogranular Au film on Si was shown to enhance the LAO activity.[28] The authors obtained grown oxidative heights up to few tens of nanometers with deposition of an appropriate thickness of gold on the surface of silicon. Such studies[23,24,28] do provide instances where the deposited Au may act as a catalyst similar to monodispersed clusters in Goodman's study.[11] However, these are studies on a collection of Au nanocrystals, where the observed catalytic performance may be additive. As such, the observation of the catalytic activity of a single isolated nanocrystal (Au or otherwise) is not common. It was of our interest to investigate the catalytic activity of Au nanocrystals in LAO, obtained by different chemical means. For this purpose, Au/SiO_x interfaces were obtained by growing Au nanocrystals from an electroless plating solution as well as by spin-coating a well-characterized Au organosol. These methods of deposition gave a fine control on the size, density and distribution of the nanocrystals compared to sputtering. Our study has shown that while Au-modified surfaces generally enhance the oxide growth, single Au nanocrystals can enhance LAO several times that observed on bare Si surface (see scheme in Figure 1).

Experimental Section

To start, an n-type Si(100) wafer was cleaned by sonicating in acetone followed by a rinse in double distilled water for 2 min. The Si substrate used has been doped to 10^{15} cm^{-3} (~5 Ω cm) in order to guarantee a sufficient conductivity of the substrate for the LAO process.[29] Electroless deposition of gold on silicon was done by dipping the wafer in a 20 mL bath containing the mixture of $KAuCl_4$ (0.8 μmoles) and aqueous HF (10 M) for ~1 s, followed by a wash in double distilled water. This resulted in the nucleation and growth of particles with a diameter of a few nanometers.[30] For a size-controlled dispersion of Au nanocrystals, an organosol containing the desired Au nanocrystals was prepared employing a procedure developed in our laboratory.[31] Briefly, metal nanocrystals were first prepared in an aqueous medium by the reduction of $HAuCl_4$ using $NaBH_4$ in the presence of dimethylsulfoxide (DMSO). This method avoids the use of a surfactant or a mineral acid while carrying out the phase-transfer of the colloid from aqueous to an organic medium. The nanocrystal diameter was in the range from 2.5 to 4 nm with a mean value of 3 nm as revealed by TEM, JEOL JEM 3010 microscope (Supporting Information, Figure S1). A 10 μL of 2 mM toluene dispersion of the nanocrystals was deposited on a freshly cleaned Si surface by spin coating at 3000 rpm. LAO patterning and subsequent imaging was performed at a relative humidity of 45%, using a Co/Cr coated tip (spring constant 2.8 Nm^{-1} and resonance frequency 75 kHz) on an AFM setup (Dimension 3100 SPM with NS-IV controller, Veeco, USA) in tapping mode. With the Si substrate held at ground potential, typically a tip bias of −12 V and a writing speed of 0.5 μm/s were employed for patterning. Uniform oxide growth was seen under these tip conditions.

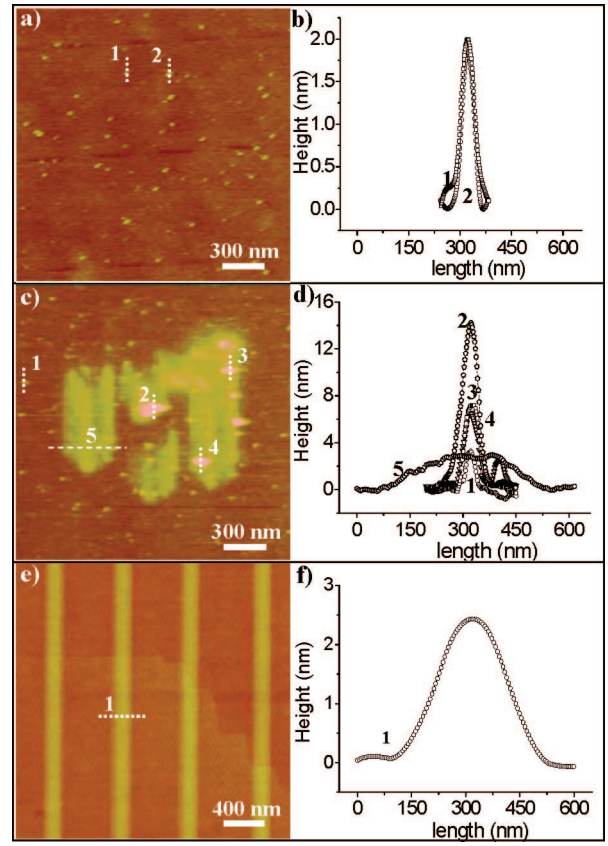

Figure 2. (a) AFM image of a Si substrate deposited with Au from a plating solution, (b) z-profiles correspoing to dashed lines numbered 1 and 2 in panel a. The image after performing LAO on this surface is shown in (c) along with the z-profiles (d) in the designated regions. LAO on bare Si substrate is shown in (e,f).

In another study, a heavily doped AFM tip (10^{-3} Ω-cm, boron doped Si) was made to carry the Au nanodeposit instead of the Si surface. This was achieved by engaging the AFM tip onto a polycarbonate substrate for 3−4 s onto a drop of the electroless plating solution. The tip was washed with distilled water and subsequently imaged by energy dispersive spectroscopy using field-emission scanning electron microscopy (FESEM) (Nova Nano 600 FESEM, FEI, Netherlands) to confirm the presence of nanoparticles. This tip was used to draw LAO patterns on bare silicon and the resulting LAO patterns were compared to those obtained with a bare tip.

Results and Discussions

The LAO process on the Au/Si surface obtained by electroless plating is compared with that on a bare Si surface in Figure 2. Figure 2a shows an AFM image of the Au-plated Si surface before oxidation. Here, Au is present on the silicon surface in the form of nanoislands with lateral dimensions between 30 to 40 nm and height ~2 nm, as shown in the z-profiles (numbered

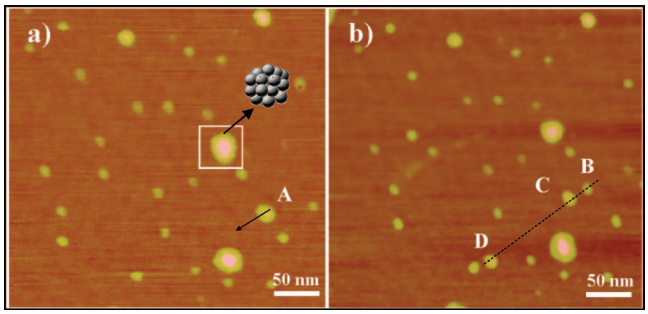

Figure 3. (a) AFM image of the Si substrate spin coated with 10 μL Au sol. A schematic of an aggregate is shown. An aggregate subjected to nanomanipulation is marked as "A". (b) Nanomanipulation of A leading to B, C, and D features. Some features corresponding to isolated nanocrystals exhibit small displacements due to surface diffusion.

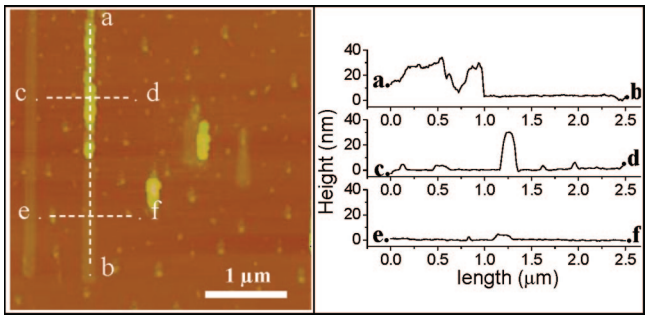

Figure 4. AFM image of an Au nanocrystal loaded Si surface after LAO, along with height profiles (Au sol loading 10 μL).

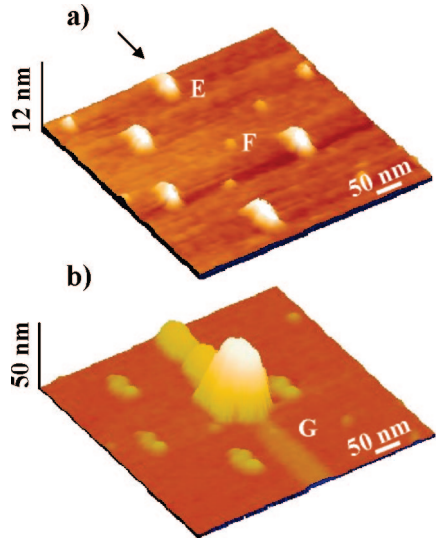

Figure 5. (a) AFM image showing several individual Au nanocrystals along with nanocrystal aggregates. (b) AFM image of the same region after performing LAO.

1 and 2) in Figure 2b. Figure 2c shows the same surface after the LAO process. The oxide patterns are somewhat broad (~250 nm) and importantly exhibit increased elevations presumably at those locations where nanocrystalline islands were present. The height of the oxide islands can be as much as 14 nm (Figure 2d, profile 2), way above the typical height of an Au deposit (see Figure 2b). Further, these heights are several times the values that one obtains by a LAO process on a bare Si surface (see Figures 2e and f). The intermittent enhancement of oxide growth observed on this surface may be due to the high aspect ratio of the Au deposits. Nevertheless, this experiment does provide evidence for the catalytic activity on a Au-modified Si surface.

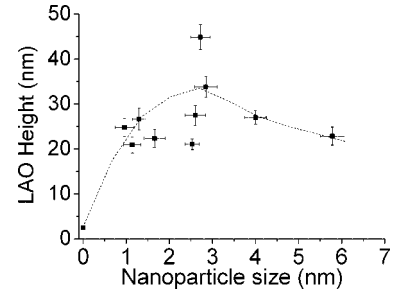

Figure 6. Variation in the height of the LAO line with the Au nanocrystal size (its height). The dashed line is to guide the eye.

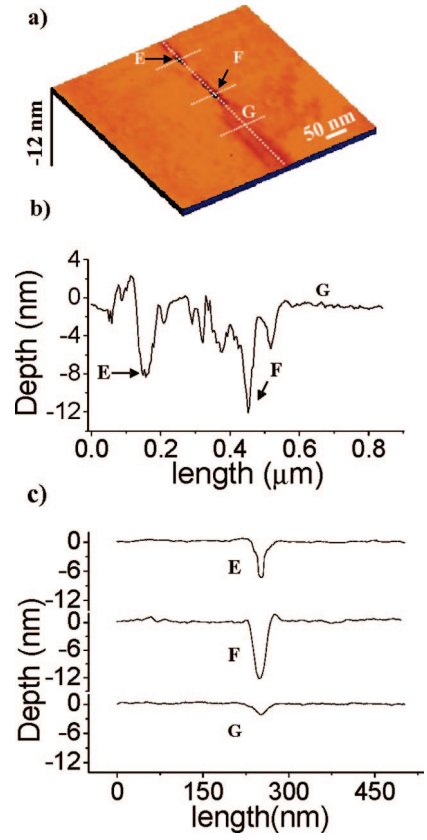

Figure 7. (a) AFM image after the surface was etched with HF. Marked pointers show deep trenches where the nanoparticles were present. (b) Profile along the trench in panel a. (c) Profiles through features E, F, and G perpendicular to the profile shown in panel b.

TABLE 1: LAO Height, Trench Depth and Apparent Volume Expansion Values for Different Features (E, F and G) in Figures 6 and 7

	E (nm)	F (nm)	G (nm)
feature height (*a*)	8	2.7	0
observed LAO height (*b*)	19	42	2.5
approximate estimated oxide height; $h = (b - a)$	11	39.3	2.5
observed trench depth (*d*)	8	13	2
apparent volume expansion $[(h + d)/d]$	2.38	4.02	2.24

In the following study, we have used well-characterized Au nanocrystals deposited on the Si surface by spin coating. The AFM image of as-deposited Au nanocrystals on Si after coating with 10 μL Au sol (Figure 3a) shows that the deposit contains many individual nanocrystals all over the surface, and some bigger aggregates. The percentage of the individual nanocrystals dispersed on the substrate is around 80%. It is apparent that

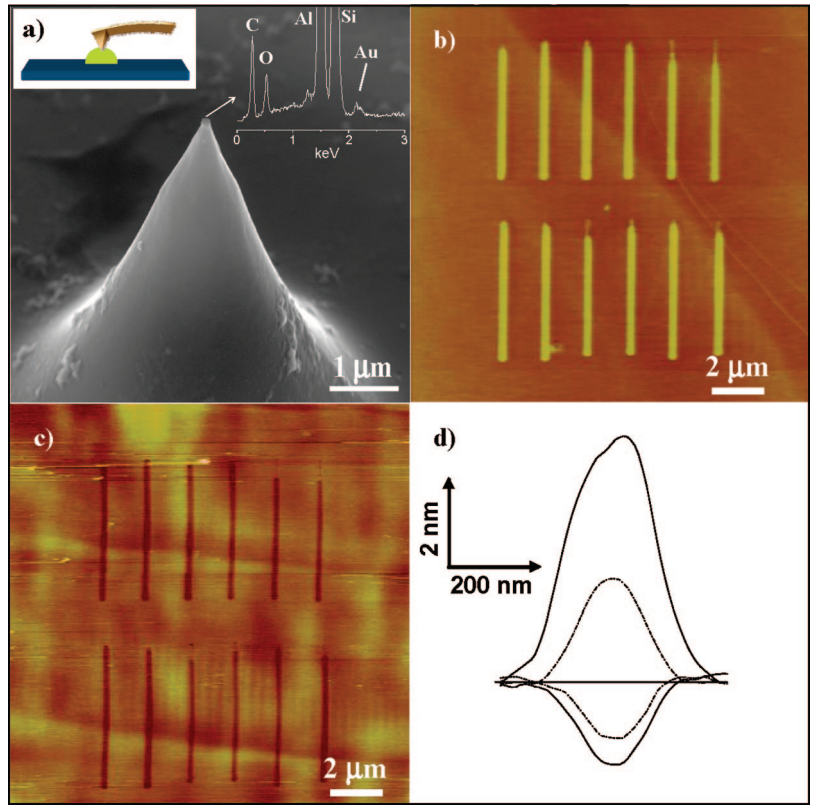

Figure 8. (a) SEM image of the Si tip after engaging it through a drop of the electroless plating solution (see schematic on the top left). The EDS spectrum is shown in the inset on the top right. (b) LAO patterns drawn with the electroplated tip. (c) Trenches formed after etching in dilute HF. (d) Profiles of the oxide protrusions and the corresponding trenches (solid lines) compared with those from an LAO performed with uncoated tip (dotted lines).

the diameter of a nanocrystal as measured by AFM (~6 nm) is somewhat larger than the TEM value (3 nm) as the former includes the thickness of the dodecanethiol ligand shell, besides tip convolution effects.[32]

In order to understand the nature of the bigger aggregates, nanomanipulation was performed with 20 nN force on the aggregate labeled "A" in Figure 3a using a Si_3N_4 tip. The aggregate was dragged along when it broke into three smaller features, labeled B, C, and D in Figure 3b. The feature B remained in the same position as the parent aggregate, while C and D are located along the stroke direction, ~50 and 250 nm away, respectively. It is thus clear that features such as A consist of loosely bound nanocrystals. Because the Si surface and its native oxide layer are hydrophilic in nature, it is understandable that the dodecanethiol-capped nanocrystals loosely bind to one another to form aggregates which may be easily broken up. What is borne out of this experiment is that the nanocrystals retain their individuality, in spite of aggregation through ligand shell interaction.[33]

We have performed LAO on Si with different Au sol loadings. We observed that with an increase in the Au loading during spin coating to 30 and 50 μL, the mean size of the aggregates increased to 13 and 40 nm, respectively, while the fraction of individual particles on the surface decreased from 70 to 40%. We have performed LAO on Si substrates with different Au loadings (30 and 50 μL of the sol). The enhancement of LAO in all cases was clearly observed (see Supporting Information, Figure S2).

Often, it proved difficult to decipher the catalytic enhancement by the nanocrystal aggregates as against contributions from isolated nanocrystals. Figure 4 contains an example of LAO performed in a region where the Si surface was predominantly covered with isolated Au nanocrystals.

The height profile along the line "ab" in Figure 4 shows regions with an oxide height as much as 25 nm, which is also affirmed by the "cd" profile perpendicular to the ab line pattern. On the other hand, the profile along "ef" contains a small feature with a height of 2.5 nm similar to an oxide pattern on bare Si. We consider the region with high LAO activity (along ab and cd profiles) to contain catalytically active Au nanocrystals. The enhancement in LAO in this case is nearly 10 times the value seen on a bare Si surface. All the above observations singularly point out that an individual Au nanocrystal on Si surface is highly active in LAO.

In Figure 5, we show LAO performed on an isolated nanocrystal. LAO was performed over the features "E" and "F" in the direction indicated by the arrow. Before oxidation, the feature E exhibits a height of 8 nm typical of an aggregate while the feature F bears a height of 2.7 nm corresponding to a single nanocrystal (Figure 5a).

A striking observation is that following LAO, a huge amount of oxide (~42 nm) is seen in the region F where an isolated nanocrystal was located (Figure 5b). Even if the oxide heap contains some pores or cavities, the volume occupied by the oxide is still remarkable. It appears that the nanocrystal is able to bring down the energy threshold for anodic oxidation due to its catalytic action, thus causing enhanced oxidation around the region. In contrast, the aggregate E produced an oxide height of ~19 nm. In this case, the native oxide interface may not be well defined and the tip-induced field may at best desorb the organic capping with the resulting agglomerate being relatively less active. In Figure 5b, we also show LAO on bare Si (G) with a typical oxide height of ~2.5 nm.[34]

The oxide heights obtained with Au nanocrystals of different sizes are shown in the plot in Figure 6. The smallest nanocrystal seen is of ~1 nm diameter giving rise to an oxide height of

~25 nm. An enhancement more than 10 times the normal LAO is clearly seen in all the cases. One may also visualize a trend, where maximum enhancement is seen for a nanocrystal size of around 3 nm. These observations are in close agreement with Goodman's findings.[12]

It is well known that the LAO oxide partly extends into the substrate.[35] When the surface shown in Figure 5b was etched in dilute HF (1:50) for 1 min, trenches of varying depths are found in the previously oxidized regions (Figure 7). While the trench corresponding to the oxide formed over the isolated nanocrystal is as deep as ~13 nm (see profiles in Figure 7b and c), the depth is only ~8 nm where the bigger aggregate E was situated. LAO on bare Si along the same line (feature G) produced a trench of ~2 nm with width corresponding to tip diameter (~40 nm). Interestingly at E and F locations, the trench width is significantly smaller (~12 nm), implying that the nanocrystal or the aggregate acts as a virtual tip, allowing high resolution etch patterns. The various height and depth values are listed in Table 1. The apparent volume expansion defined as the ratio, LAO oxide height plus the trench depth divided by the trench depth,[36] is also shown for the three features E, F, and G. It is clear that in the case of Au-catalyzed process, the oxide formed is relatively less dense. The observed trench depths and the profiles clearly point out the higher volume of Si used up in the catalyzed process.

Further, we designed an experiment where instead of the Si surface, the AFM tip was made to carry the Au nanodeposit (Figure 8). For this purpose, a Si tip was used and the Au deposition was achieved by engaging it with a polycarbonate surface through a drop of the plating solution. SEM imaging revealed the presence of a small deposit (~10 nm) at the tip (Figure 8a), which was confirmed by collecting EDS data (see inset in Figure 8a). The Au-coated tip routinely produced bright oxide lines under typical bias of −12 V. Following etching in dilute HF, we observed well-formed trenches (Figure 8c). In Figure 8d, we show typical z-profiles of the oxide lines and the trenches along with those from normal LAO performed with an uncoated Si tip. We readily observe that the oxide lines produced by the Au-coated tip exhibit a height of ~6 nm, close to three times the height seen in normal LAO. Similarly the trench depths are typically 2.2 nm as compared to 1.8 nm from normal LAO.

The following insight may be obtained from the above observations. In the LAO process, the intense electric field from the AFM tip ionizes the water molecules in the meniscus inducing oxidation locally. In the presence of gold either on the Si surface in the form of a nanocrystal on the Si surface, or as a nanodeposit at the apex of the tip, the formation of hydroxyl ions may become more facile due to surface oxygens. To bring about local oxidation, the Si surface is covered with the native oxide (SiO_x) and the deposited Au nanoparticles are likely to carry surface AuO_x species. The AuO_x bond increases the density of hydroxyl ions locally. During LAO, the diffusion of these hydroxyl ions into the Si lattice would increase, thereby enhancing the oxidation.

Conclusions

In summary, enhancement in the local anodic oxidation (LAO) of the Si surface in the presence of nanoscale gold was observed and compared with that of bare silicon. Au nanodeposits obtained by dipping the Si substrate in an electroless plating solution produced oxide islands with increased heights. The Au nanocrystals deposited from a colloidal sol produced distinct effects. Individual Au nanocrystals (~3 nm) showed high catalytic activity, leading to large oxide height (~42 nm) in contrast to ~2.5 nm oxide height on bare Si. Etch profiles obtained in the region of the oxide were unusually deep (~13 nm) compared to LAO done on bare Si (~2 nm). The oxide height obtained with nanocrystal aggregates or with sputtered films is relatively less, indicating only a mild enhancement. Another independent observation of the catalytic action of nanogold comes from our study of LAO performed with a Au-coated tip on a bare Si surface. In this case, well-defined oxide line patterns with 6 nm height could be easily drawn. This study unequivocally demonstrates the high catalytic activity of individual Au nanocrystals hitherto not observed.

Acknowledgment. The authors thank Professor C. N. R. Rao for encouragement. They acknowledge support from the Indo-Italian POC in S&T 2005−2007. They are thankful to Department of Science and Technology for support and to the Veeco-India Nano Laboratory for providing the AFM facility. They also thank Ms. Supreet for assistance.

Supporting Information Available: TEM image of Au nanocrystals and AFM image of an enhanced LAO observed on Si with different particle loadings. This material is available free of charge via the Internet at http://pubs.acs.org.

References and Notes

(1) Haruta, M.; Kobayashi, T.; Tsubota, S.; Nakahara, Y. *Chem. Express* **1988**, *5*, 349–357.
(2) Haruta, M. *Catal. Today* **1997**, *36*, 153–166.
(3) Iizukaa, Y.; Fujikia, H.; Yamauchia, N.; Chijiiwaa, T.; Araia, S.; Tsubota, S.; Haruta, M. *Catal. Today* **1997**, *36*, 115–123.
(4) Grunwaldt, J. D.; Baiker, A. *J. Phys. Chem. B* **1999**, *103*, 1002–1012.
(5) Vinod, C. P., Kulkarni, G. U.; Rao, C. N. R. Nanoscale catalysis by gold. *Surface Chemistry and Catalysis*; Carley, A., Davies, P., Hutchings G., Spencer, M., Eds.; Kluwer Academic/Plenum Publishers: New York, 2002; pp 191−206.
(6) Hashmi, S. K.; Hutchings, G. J. *Angew. Chem., Int. Ed.* **2006**, *45*, 7896–7936.
(7) Edwards, P. P.; Thomas, J. M. *Angew. Chem., Int. Ed.* **2007**, *46*, 5480–5486.
(8) Yan, W.; Brown, S.; Pan, Z.; Mahurin, S. M.; Overbury, S. H.; Dai, S. *Angew. Chem., Int. Ed.* **2006**, *45*, 3614–3618.
(9) Hashmi, S. K. *Chem. Rev.* **2007**, *107*, 3180–3211.
(10) Min, B. K.; Friend, C. M. *Chem. Rev.* **2007**, *107*, 2709–2724.
(11) Valden, M.; Lai, X.; Goodman, D. W. *Science* **1998**, *281*, 1647–1650.
(12) Chen, M. S.; Goodman, D. W. *Science* **2004**, *306*, 252–255.
(13) Hammer, B.; Nørskov, J. K. *Nature* **2002**, *376*, 238–240.
(14) Daté, M.; Okumura, M.; Tsubota, S.; Haruta, M. *Angew. Chem., Int. Ed.* **2004**, *43*, 2129–2132.
(15) Bore, M. T.; Pham, H. N.; Switzer, E. E.; Ward, T. L.; Fukuoka, A.; Datye, A. K. *J. Phys. Chem. B* **2005**, *109*, 2873–2880.
(16) Bethke, G. K.; Kung, H. H. *Appl. Catal., A* **2000**, *43*, 194–195.
(17) Costello, C. K.; Kung, M. C.; Oh, H. S.; Wang, Y.; Kung, H. H. *Appl. Catal., A* **2002**, *232*, 159–168.
(18) Carrettin, S.; Concepcion, P.; Corma, A.; Nieto, J. M. L.; Puntes, V. F. *Angew. Chem., Int. Ed.* **2004**, *43*, 2538–2540.
(19) Guzman, J.; Gates, B. C. *J. Phys. Chem. B* **2002**, *106*, 7659–7665.
(20) Lopez, N.; Nørskov, J. K. *J. Am. Chem. Soc.* **2002**, *124*, 11262–11263.
(21) Yoon, B.; Hakkinen, H.; Landman, U.; Worz, A. S.; Antonietti, J. M.; Abbet, S.; Judai, K.; Heiz, U. *Science* **2005**, *307*, 403.
(22) Fu, Q.; Saltsburg, H.; Flytzani-Stephanopoulos, M. *Science* **2003**, *301*, 935.
(23) Robinson, J. T.; Evans, P. G.; Liddle, J. A.; Dubon, O. D. *Nano Lett.* **2007**, *7*, 2009–2013.
(24) Robinson, J. T.; Ratto, F.; Moutanabbir, O.; Heun, S.; Locatelli, A.; Mentes, T. O.; Aballe, L.; Dubon, O. *Nano Lett.* **2007**, *7*, 2655–2659.
(25) Sugimura, H.; Uchida, T.; Kitamura, N.; Masuhara, H. *J. Phys. Chem.* **1994**, *98*, 4352.
(26) Avouris, Ph.; Martel, R.; Hertel, T.; Sandstrom, R. *Appl. Phys. A* **1998**, *66*, S659.
(27) Dagata, J. A.; Schneir, J.; Harary, H. H.; Evans, C. J.; Postek, M. T.; Bennett, J. *Appl. Phys. Lett.* **1990**, *56*, 2001–2002.

(28) Hwang, J. S.; You, Z. Y.; Lin, S. Y.; Hu, Z. S.; Wu, C. T.; Chen, C. W. *Appl. Phys. Lett.* **2005**, *86*, 161901–161903.

(29) Dagata, J. A.; Inoue, T.; Itoh, J.; Matsumoto, K.; Yokoyama, H. *J. Appl. Phys.* **1998**, *84*, 6891–6900.

(30) Bhuvana, T.; Kulkarni, G. U. *Bull. Mater. Sci.* **2006**, *29*, 505–508.

(31) Vijaykumar, T.; Sanketh, R.; Kulkarni, G. U. *Chem. Phys. Lett.* **2007**, *436*, 167–170.

(32) Tranchida, D.; Piccarolo, S.; Deblieck, R. A. C. *Meas. Sci. Technol.* **2006**, *17*, 2630–2636.

(33) Thomas, P. J.; Agrawal, V. V.; Saravanan, P.; Kulkarni, G. U.; Rao, C. N. R. *J. Phys. Chem. B* **2003**, *107*, 7391–7395.

(34) Vijaykumar, T.; Kulkarni, G. U. *Solid State Commun.* **2007**, *142*, 89–93.

(35) Fontaine, P. A.; Dubois, E.; Stiévenard, D. *J. Appl. Phys.* **1998**, *84*, 1776–1781.

(36) Hattori, T.; Ejiri, Y.; Saito, K.; Yasutake, M. *J. Vac. Sci. Technol., A* **1994**, *12*, 2586–2590.

JP804545S